https://doi.org/10.2478/acph-2025-0021

Original research paper

Formulation and characterization of advanced nanostructured lipid carriers (NLC) incorporating coenzyme Q10 and licorice extract to explore their synergistic antioxidant and antityrosinase effects

HODA ATAPOUR-MASHHAD[a,1,2,*]
AFSANEH HOSEINSALARI[a,3]
ZAHRA TAYARANI-NAJARAN[4,5]
JAVAD ASILI[6]
ARMITA SEDIGHIDARIJANI[1]
SHIVA GOLMOHAMMADZADEH[1,2,*]

[1] *Department of Pharmaceutics, Faculty of Pharmacy, Mashhad University of Medical Sciences, Mashhad, Iran*
[2] *Nanotechnology Research Center, Pharmaceutical Technology Institute, Mashhad University of Medical Sciences, Mashhad, Iran*
[3] *Department of Pharmacognosy, Faculty of Pharmacy, Tehran University of Medical Sciences, Tehran, Iran*
[4] *Medical Toxicology Research Center, Mashhad University of Medical Sciences, Mashhad, Iran*
[5] *Targeted Drug Delivery Research Center, Pharmaceutical Technology Institute, Mashhad University of Medical Sciences, Mashhad, Iran*
[6] *Department of Pharmacognosy, Faculty of Pharmacy, Mashhad University of Medical Sciences, Mashhad, Iran*

[a] These authors contributed equally to this paper.
* Correspondence; e-mails: Golmohamadzadehsh@mums.ac.ir, Asal.Atapour@gmail.com

ABSTRACT

The development of novel nanostructured lipid carrier (NLC) formulations incorporating coenzyme Q10 (Co-Q10) and licorice extract (LE) was investigated to evaluate their synergistic effects as an antioxidant and antityrosinase agent, respectively. The ethyl acetate fraction of licorice extract (LE), containing 6.59 mg g^{-1} of liquiritin, and 31.71 mg g^{-1} of glabridin, was successfully encapsulated with Co-Q10 in the NLC matrix. Characterization of the formulations (F1 to F8) demonstrated favorable surface properties, with Z-average sizes ranging from 146 to 248 nm, polydispersity indices (PDI) between 0.21 and 0.27; and zeta potentials from –5 to –15 mV, indicating acceptable physicochemical stability over six months and entrapment efficiency (*EE* %) exceeding 69 %. Furthermore, these formulations significantly reduced reactive oxygen species (ROS) levels and tyrosinase activity in cell assays compared to controls, without exhibiting cytotoxic effects. Notably, the NLCs with a 1:1, 1:0.5, and 0.5:1 ratio of Co-Q10 to LE showed enhanced efficacy compared to individual components, with formulation F8 (Co-Q10/LE: 0.5/1) displaying the most pronounced synergistic effect. These findings indicate that Co-Q10/LE-NLC formulations exhibit stable physicochemical properties, making them suitable for topical applications targeting antiaging and skin-lightening benefits.

Keywords: coenzyme Q10, licorice extraction, NLC, sROS inhibition, antityrosinase, synergistic effect

Accepted June 5, 2025
Published online June 6, 2025

INTRODUCTION

Skin aging is a complex process influenced by both internal and external factors (1). Among these, ultraviolet (UV) radiation plays a significant role in accelerating aging; UV rays, including UVA and UVB, penetrate the skin and generate reactive oxygen species (ROS) (2), leading to oxidative stress, damaging essential cellular components such as DNA, proteins, and lipids (3). As a result, collagen breakdown and reduced procollagen and hyaluronic acid production are impaired, contributing to wrinkles and reduced skin elasticity (4). Another consequence of UV-induced damage is hyperpigmentation. UV rays serve as the primary physiological trigger for melanogenesis, influencing melanocytes directly or indirectly through the release of factors such as α-MSH (α-melanocyte-stimulating hormone) (5). Although melanin offers protection against UV rays (6), excessive production can lead to pigmentation issues (7). Tyrosinase, an enzyme dependent on copper, is crucial for melanin synthesis and catalyzes several key steps in this process (8). Inhibiting tyrosinase activity can reduce melanin synthesis and prevent pigmentation (9).

Antioxidants like niacinamide (vitamin B3), vitamin E, vitamin C, resveratrol, glutathione, curcumin, and coenzyme Q10 (Co-Q10) are renowned for their ability to enhance collagen production, protect against UV damage, and offer anti-inflammatory benefits (10). These compounds improve skin elasticity and help reduce signs of aging (10). Among antioxidants, Co-Q10 is unique because it is naturally synthesized within cells (11). It is essential for energy production and helps safeguard against oxidative damage (12), inhibits lipid peroxidation and shields tissues from ROS (12). Regretfully, the Co-Q10 amount in the skin decreases with age, and using Co-Q10-containing products with high skin penetration could supply the skin's needs (13). Co-Q10's limited water solubility (0.193 μg mL^{-1}) (14), high lipophilicity (log$P$ > 10), substantial molecular weight (863.36 g mol^{-1}), and susceptibility to degradation from light exposure hinder its effectiveness in medicine and its ability to penetrate the skin (15).

Licorice root from *Glycyrrhiza glabra* L. is valued for its medicinal properties and is native to Asian regions, such as Iran and some Mediterranean countries (16). It contains various beneficial compounds like triterpenoid saponins, flavanones, chalcones, flavones, isoflavones, isoflavanes, and coumarins, which order antibacterial, antiviral, anti-inflammatory, antidiabetic and antioxidant properties (17). Among these phytochemicals of licorice, glabridin and liquiritin are particularly noted for their skin-lightening properties (18). They have a log$P$ value of less than 5 (19). Liquiritin a flavonoid with a flavanone glycoside, disperses melanin and enhances its elimination from the epidermis (20). It also reduces inflammation and erythema caused by UV rays (21). Glabridin, another flavonoid with a pyranoisoflavan structure, is a potent tyrosinase inhibitor, exhibiting skin-whitening 16 times stronger than hydroquinone (22). However, glabridin has poor skin permeability and chemical stability (23). Therefore, a formulation containing Co-Q10 and licorice extract (LE) is required to provide chemical stability and increase bioavailability.

Nanostructured lipid carriers (NLC) are innovative lipid-based nanoparticles designed to enhance the delivery of active substances in topical formulations (10). They consist of a blend of solid lipids, liquid lipids, and surfactants that collaborate to enhance the stability and effectiveness of the encapsulated substances (10). NLC formulations in topical products can significantly increase the chemical stability of active ingredients, lower toxicity levels, and boost skin hydration thanks to their occlusive properties (24).

This study explores the creation of innovative skincare products by formulating new NLCs that incorporate a combination of Co-Q10 (an antiaging agent) and LE (a skin-lightening agent) in ratios of 1/1, 1/0.5, and 0.5/1. The research investigates their synergistic effects through surface characterization, long-term stability assessments, entrapment efficiency measurements, modulation of reactive oxygen species (ROS) levels, inhibition of melanin production, and antityrosinase activities.

EXPERIMENTAL

Materials

Materials used in this study include glyceryl behenate (Compritol® 888 ATO) and glyceryl palmitostearate (Precirol® ATO 5) generously provided by Gattefossé (Pvt. Ltd., France). Glyceryl tripalmitate (tripalmitin) was purchased from Fluka (Germany), while glycerol monostearate (GMS), cetyl palmitate, dimethyl sulfoxide (DMSO), poloxamer 188, Span® 80, N-acetylcysteine (NAC), kojic acid, phenylmethanesulfonyl fluoride (PMSF), L-3,4-dihydroxyphenylalanine (L-DOPA), and 2',7'-dichlorofluorescein diacetate (DCFH-DA) from Sigma-Aldrich Co. (Germany); stearic acid and cetyl alcohol from Merck (Germany), and HPLC grade coenzyme Q10 (purity: > 98 %) was obtained from Tinab Shimi Khavarmianeh (Mashhad, Iran); HPLC grade ridin glabridin and liquiritin (purity: > 98 %) were acquired from Nanjing Dilger Medical Technology (China), and Tween 80 was aquired from Kimyagaran Emrooz (Iran), oleic acid and medium-chain triglyceride (MCT) were obtained from Oxin Chemistry Company (Iran); methanol (analytical grade) and ethyl acetate were sourced from Dr. Mojallali Industrial Chemical Complex Co. (Iran), HPLC grade solvents, methanol and acetonitrile were acquired from Tedia (USA); tetrahydrofuran (THF) was sourced from CARLO ERBA (Germany). All chemicals utilized were of analytical grade, with a purity greater than 98 %.

The fetal calf serum (FBS) and Dulbecco's Modified Eagle Medium (DMEM) were obtained from Gibco, (USA). Resazurin (AlamarBlue®) was sourced from BioSource Invitrogen; while doxorubicin (DOX) in a concentration of 10 mg *per* 5 mL was acquired from Ebewe.

Plant material collection and authentication

The roots of *G. glabra* were acquired from Shirin Darou Company (Iran), on May 9, 2021. Following authentication and the assignment of the collection number (PMP-1255), voucher specimens were lodged in the Herbarium of the Department of Pharmacognosy at Tehran University of Medical Sciences, Tehran, Iran, for documentation and verification purposes.

Preparation of licorice extract

The dried roots were finely crushed using an electric mill before extraction. About 200 g of the ground roots were then placed in an Erlenmeyer flask and subjected to maceration thrice with methanol at 24-, 48- and 72-hour intervals (25). Following maceration, the concentrated methanolic extract was fractionated using ethyl acetate three times. The solvent was separated with a rotary evaporator. The residual solvent was eliminated using a Laminar Flow Hood and a freeze-dryer. Finally, the ethyl acetate fraction was prepared to be capsulated by NLC formulations.

HPLC analysis

Glabridin and liquiritin, used as quantitative standards for LE, together with Co-Q10, were analyzed using high-pressure liquid chromatography (HPLC) (Shimadzu, Japan). The HPLC system was supplied with a C18 reversed-phase column (5 μm, 250 × 4.6 mm; Perfect Sil Target ODS-3), a solvent delivery unit (LC-

20A pump), and a UV-Vis detector (SPD-20A), following the guidelines outlined in USP35. All samples were injected using a fixed 20 µL loop with a Rheodyne® Model 3725i valve. For the analysis of glabridin and liquiritin , a mobile phase that included acetonitrile and water was utilized at a flow rate of 1 mL min^{-1}, considering the polarity of these compounds (19). A gradient solvent system ranging from 10:90 to 90:10 (*V/V*) acetonitrile and water was implemented, as detailed in Table S1 of the Supplementary material. The UV wavelength for glabridin detection was 280 nm (26), and for liquiritin (27), it was 276 nm. The retention times for glabridin and liquiritin were approximately 38–39 min and 16–17 min, respectively. The standard curves were constructed at six points with 0.03–1 mg mL^{-1} concentration ranges.

To quantify Co-Q10, a Lichrospher C8 column (5 µm, 4.6 mm ID, 25 cm; Hanbag, China) was employed. The mobile phase used was an isocratic solvent system with a composition of 95:5 (*V/V*) methanol and tetrahydrofuran. The UV detection was set to a wavelength of 275 nm, with Co-Q10 exhibiting a retention time of 5 to 6 minutes. A standard six-point calibration curve was established at concentrations ranging from 0.06 to 2 mg mL^{-1} (28). This procedure was carried out in triplicate for each compound.

Standard and sample solution preparation procedures. – Stock solutions were prepared for glabridin and liquiritin at a concentration of 1 mg mL^{-1} in methanol, while a stock solution for Co-Q10 was made at a concentration of 2 mg mL^{-1} in a mixture of methanol and THF (50:50). These solutions served as the basis for constructing the calibration curves.

Various aliquot concentrations were obtained by diluting the initial stock solutions. The resulting concentrations were as follows: glabridin and liquiritin: ranging from 1 to 0.0312 mg mL^{-1}, Co-Q10: ranging from 2 to 0.0625 mg mL^{-1}. Before each injection, a 0.22-micron syringe filter was used for standard and sample solutions. Samples were injected at constant volume using a Rheodyne® injector Model 3725i valve equipped with a 20 µL fixed loop.

Solubility test of active ingredients

To develop an effective formulation of NLC containing Co-Q10 and LE, the solubility of the active ingredients in several solid lipids, including Precirol, Tripalmitine, Compritol, cetyl palmitate, stearic acid, and GMS, as well as in liquid lipids like oleic acid and MCT oil, was assessed. Additionally, surfactants such as Tween 80, Poloxamer 188, and Span 80 were evaluated. The solubility tests were conducted based on the NLC formulation, for instance, 50 mg of LE was dissolved in 350 mg of each solid lipid.

The solutions were heated in a water bath to around 10 °C in excess of the melting point of the lipids and maintained at this temperature while being stirred continuously for 10 minutes. The criteria for determining the dissolution of the active ingredients within the lipid and surfactant matrix were based on the clarity of the resulting solution and lack of any sedimentation.

Formulation of Co-Q10/LE-NLCs

Initially, 50 mg of LE was combined with 100 µL of an equal ratio of ethanol/propylene glycol, then heated to 75 °C in a water bath. Following this, the solid, and liquid lipids and surfactant, (as specified in Table I) were added and melted a temperature about 10 °C beyond the melting point of solid lipid. Co-Q10 was then incorporated into the lipid phase and agitated until dissolved at approximately 1 min. Simultaneously, double-distilled water was subjected to identical thermal conditions as the lipid mixture. The phases were combined and homogenized using an Ultra-Turrex (Heidolph DIAK) in three sequential steps: 1.5 minutes at 18,000 rpm, followed by 1.5 minutes at 23,000 rpm, and finally 1 min at 28,000 rpm. During the homogenization process, the temperature of the mixture was maintained approximately 5 ˚C beyond the melting point of the solid lipid (approximately 75 °C). The mixture underwent sonication for seven cycles,

each lasting 60 seconds, with a 15-second resting period between cycles, using a Bransonic sonicator probe (USA) (28). Subsequently, the solution was gradually cooled to ambient temperature, leading to the formation of a nanoemulsion (28).

The exact amounts of active ingredients in the NLCs (equivalent amounts in percentage, moles and µg mL^{-1}) are given in Table S3 in the supplementary file. During NLC preparation, the licorice extract's high melting point (140 ± 2 °C) reduces the risk of degradation at the process temperature (70 °C). Earlier research has investigated the compatibility of Co-Q10 in NLC and SLN preparations, confirming its suitability for the process (29). This suggests that the NLC preparation process for licorice extract and Co-Q10 is likely to be stable and effective.

Physicochemical characterization of the NLC formulations

The Z-average size, polydispersity index (PDI), and zeta potential were assessed using photon correlation spectroscopy (PCS) with a Zetasizer/Nano-ZS90 instrument from Malvern, UK. Measurements were taken at a 90° angle in 10 mm diameter cells at a temperature of 25 °C, with each measurement conducted in triplicte. Each measurement was repeated three times. In advance of analyzing particle size, the aqueous mixture of the NLC formulation was adjusted with distilled water to achieve the appropriate concentration (30).

Transmission electron microscopy (TEM) analysis. – The selected Co-Q10/LE-NLC (F6) feature was observed using TEM (LEO 912 AB, ZEISS, German). Before experimentation, the specimen underwent a 1:50 (*V/V*) dilution with deionized water. The diluted solution was dropped on the carbon-coated copper grid and then stained with 2 % uranyl acetate solution. After staining, the grid was left to dry at room temperature (31).

Thermal analysis of materials using differential scanning calorimetry. – Thermal analysis of freeze-dried Co-Q10, solid lipid, blank NLC (drug-free), and Co-Q10/LE-NLC formulations was performed using a Differential Scanning Calorimeter (METTLER TOLEDO DSC822e, Gießen, Germany). Each sample, weighing 3 mg, was loaded into a 40 µL aluminum DSC pan and sealed before being with the DSC instrument (32).

Key parameters such as melting point, onset temperature, and enthalpy were evaluated using STARe software. The DSC analysis was conducted over a temperature range of 0–200 °C at a heating rate of 10 °C min^{-1} under a nitrogen flow of 50 mL^{-1} min (33).

Analysis using fourier transform infrared spectroscopy. – Fourier transform infrared (FT-IR) spectra were found using a Thermo Nicolet AVATAR 370 FTIR. Some of the freeze-dried NLC was mixed with KBr salt and compressed to form a transparent disk, which was then scanned in the region of 400–4000 cm^{-1} (34).

Entrapment efficiency (EE) %

To measure the *EE* %, an ultrafiltration Falcon (Amicon Ultra 30 kDa MWCO, Millipore, USA) was utilized to separate free active ingredients from the NLC lipid matrix (28). Approximately 2 mL of NLC formulation was placed into a filter tube, and centrifuged for 10 minutes at 13,000 rpm and 4 ˚C using a Remi Elektrotechnik Ltd. centrifuge from Maharashtra, India. Direct and indirect methods were applied to assess the *EE* %. The indirect method involved analyzing the filtrate that passed through the filter membrane using HPLC. In the direct method, 50 µL of the sample retained on the filter was dissolved in a 50:50 mixture of methanol and tetrahydrofuran at 50 °C for one minute. The solution was subsequently permitted to sit at room temperature for two hours to facilitate lipid sedimentation. Following this, the sample was

centrifuged for 10 minutes at 13,000 rpm and 4 °C, and the upper clear liquid was analyzed using the HPLC system. The *EE* % was calculated using the formula:

$$EE\ \% = \frac{C_{\mathrm{E}}}{C_{\mathrm{T}}} \times 100$$

where C_T represents the total amount of Co-Q10/LE present in the system, and C_E indicates the amount of Co-Q10/LE found in the prepared sample.

The analysis methods for Co-Q10 and LE are detailed in the HPLC analysis section.

Investigating stability over time

All formulated NLCs were stored in siliconized glass vials at temperatures of 4, 25, and 40 °C to evaluate various stability parameters, including color variations, uniformity, and phase separation at the 1st, 3rd, and 6th months. Concurrently, the Z-average size, PDI, and zeta potential were measured (Table III) (35).

Cellular growth and maintenance

The murine melanoma cell line B16F10 was sourced from the Pasteur Institute located in Tehran, Iran. These cells were cultured in DMEM supplemented with 10 % (*V/V*) fetal bovine serum (FBS), along with 100 units mL^{-1} of penicillin, and 100 µg mL^{-1} of streptomycin. The culture conditions were kept in a humidified environment at 37 °C with 5 % CO_2 and 90 % humidity.

All formulations were freshly prepared prior to each experiment, ensuring that the concentration of NLC in the culture media remained below 1 % (*V/V*) (36). Given the relative solubility of Co-Q10 in alcohols, a stock solution was created using THF solvent before each test, which was then diluted in the culture medium to provide free Co-Q10.

Assessment of cell viability. – The cytotoxicity effect of NLC formulations and their protective roles against H_2O_2 were evaluated using a modified MTT assay. In this procedure, B16F10 cells (10^4 cells *per* well) were plated in a 96-well format and allowed to incubate for 24 hours. After this, the cells were treated a concentration of 1 % (*V/V*) of NLC formulations in cell culture media for a duration of 24 hours. Following the removal of the culture medium, a solution containing 10 % MTT (5 mg mL^{-1}) was permitted to the wells, and the cells were incubated for a further four hours. The MTT solution was then discarded, and 100 µL of DMSO was introduced to dissolve the formed formazan crystals. Cell viability for each treatment concentration was assessed in triplicate at a wavelength of 570 nm, using doxorubicin (DOX) at 5 µg mL^{-1} as a positive control and untreated cells as a negative control.

Cellular ROS level determination. – 2',7'-dichlorofluorescein diacetate (DCFH-DA) is a prominent reagent utilized for assessing oxidative stress levels (37). This compound is capable of permeating cell membranes and is hydrolyzed to the DCFH carboxylate anion. Upon undergoing two-electron oxidation, DCFH is converted into dichlorofluorescein (DCF), which exhibits fluorescence (37). To measure reactive oxygen species (ROS) levels, DCFH-DA was employed in this study. Approximately 10^4 of B16F10 cells were plated in a 96-well format and pretreated for 24 hours with various treatments, including free Co-Q10, lipid carrier blank, Co-Q10/LE-loaded NLC formulations (ranging from 6 to 50 µg mL^{-1}), and N-acetylcysteine (NAC) as a positive control. Following this, 10 µmol L^{-1} DCFH-DA was introduced to the cells, which were then exposed to H_2O_2 (10 mmol L^{-1}) at 37 °C for 90 minutes. The fluorescence intensity of DCF was measured at an excitation wavelength of 485 nm and an emission wavelength of 530 nm employing a fluorescent microplate reader (VICTOR X5, PerkinElmer, USA) (38).

Quantitative analysis of melanin. – B16F10 cells (10^5 cells/well) were cultivated in a 12-well plate and treated with varying concentrations of NLC formulations alongside kojic acid as a positive control, followed by a 24-hour incubation. After treatment, the cells were detached through trypsinization and washed with PBS. Subsequently, a 2 mol L^{-1} NaOH solution was added, and the plate was incubated at 100 °C for 30 minutes. The melanin levels in the treated cells were then quantified at 405 nm using a Synergy H4 Hybrid Multi-Mode Microplate Reader from BioTek (USA) (39).

Tyrosinase activity assessment in cellular models. – Cellular tyrosinase activity was assessed using a spectrophotometric method that measures the oxidation of DOPA to dopachrome (40). This assay helps determine the effectiveness of compounds in inhibiting the melanogenesis pathway by preventing this conversion. B16F10 cells were cultured and treated for melanin quantification, then washed with PBS and detached using trypsin. The cell contents were centrifuged (at 1100 rpm for 7 minutes), washed again, and lysed in a buffer included 0.1 mmol L^{-1} phenylmethylsulfonyl fluoride (PMSF), 1 % Triton X-100, and a 100 mmol L^{-1} sodium phosphate buffer adjusted to pH 6.8, employing a freeze-thaw method for effective cell disruption. PMSF was replenished every 30 minutes due to its limited half-life. The resulting lysate underwent centrifugation at 10,000 rpm for 20 minutes at a temperature of 4 °C. After this, 100 µL of the supernatant was combined with an equal volume of 5 mmol L^{-1} DOPA in a 96-well plate and incubated at 37 °C for two hours. The absorbance was then measured at 475 nm using a Synergy H4 Hybrid Multi-Mode Microplate Reader from BioTek (USA).

Data analysis

Statistical analysis was performed using One-way ANOVA (GraphPad Prism 9.0; GraphPad Software, Inc., USA). A significance level of $p < 0.05$ was established for determining statistical significance. Isobolographic analysis was conducted with CalcuSyn software v. 2. 1.

RESULTS AND DISCUSSION

Co-Q10 is the sole lipophilic antioxidant produced by human cells (11). The root extracts, specifically methanolic and ethyl acetate, contain polyphenols, terpenoids, flavonoids, saponins, and carbohydrate sugars (41). Compounds such as glycyrrhizic acid, glycyrrhizin, formononetin, glabridin, liquiritin, n-coumaric acid, luteolin-7-glucoside, acacetin, apigenin-7-*O*-glucoside, chicoric acid, and hesperetin have been reported in methanolic root extract, while glabrene, glabridin, hispaglabridin A and B, glabrone and some derivatives have been found in ethyl acetate root extract (41). Also, it has been reported that non-polar solvents like ethyl acetate are ideal for extracting specific compounds such as glabridin from natural sources like licorice roots (42). The phytochemical profile of 25 licorice roots collected from various regions of Iran was investigated, and the levels of glycyrrhizic acid, glabridin, liquiritin, and liquiritigenin in the hydroalcoholic extract (in 80 % methanolic extract) were measured. The quantities of these compounds varied among roots from different areas, with glycyrrhizic acid generally being present in higher amounts than the other compounds (43). The active ingredients in the extract may produce synergistic effects in both antioxidant and antityrosinase activities.

Evaluation using HPLC techniques

Fig. 1 displays the HPLC chromatograms for glabridin, liquiritin, and Co-Q10. The linear equations, limit of detection (*LOD*), limit of quantification (*LOQ*), and the squared correlation coefficients (R^2) for each compound are reported in Table S2 (Supplementary material). The calibration curves were generated using Microsoft Excel 2016, and the mentioned parameters were obtained by the LINEST function.

As explained in the extract preparation section, a methanolic extract was prepared initially, and then an ethyl acetate fraction was obtained to concentrate the target compounds. According to the analytical HPLC results, the methanolic extract contains 8.21 mg g^{-1} of liquiritin 11.51 mg g^{-1} of glabridin, and the ethyl acetate fraction contains 6.59 mg g^{-1} of liquiritin, and 31.71 mg g^{-1} of glabridin. Therefore, the ethyl acetate fraction containing higher concentrations of glabridin as a tyrosinase inhibitor was selected for encapsulation in NLC.

The HPLC chromatogram of the ethyl acetate fraction is shown in Fig. 1, liquiritin exhibited a shorter retention time than glabridin due to its more polar structure.

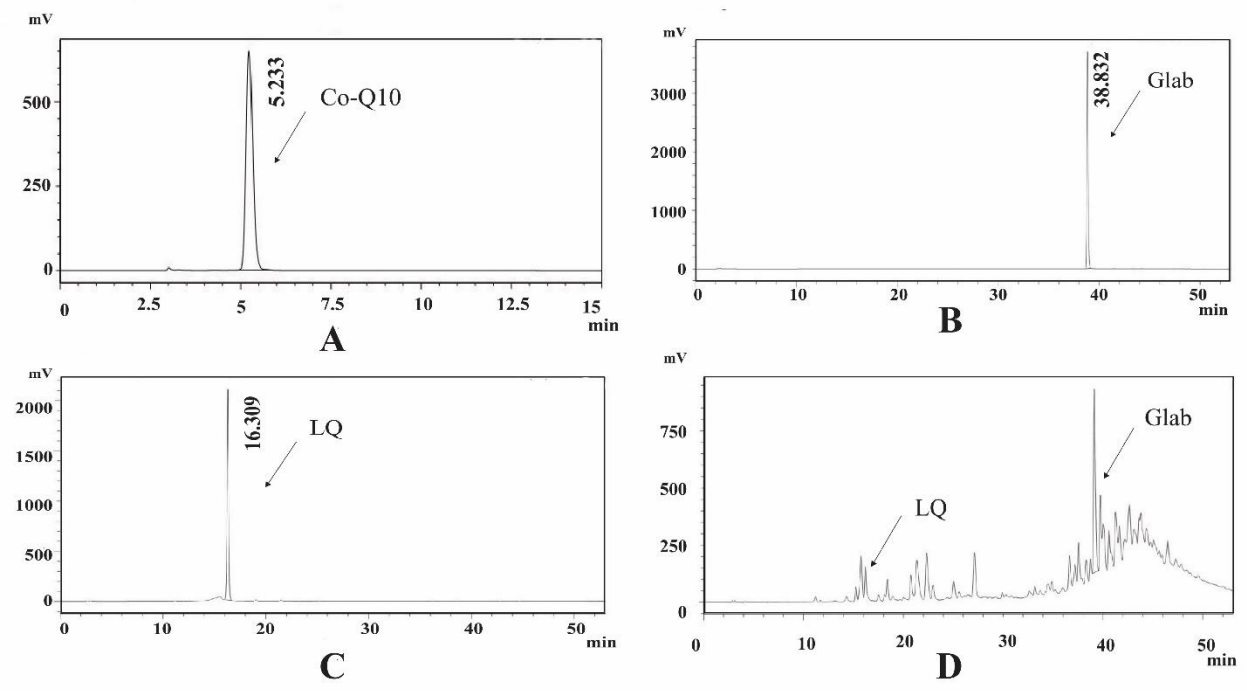

Fig. 1. The HPLC chromatogram of the standard solution of: a) Co-Q10 (1 mg mL^{-1}); b) glabridin (Glab) (1 mg mL^{-1}); c) (LQ) (1 mg mL^{-1}, and d) licorice extract (ethyl acetate fraction (10 mg mL^{-1}).

Optimization of Co-Q10/LE-NLCs formula

According to the solubility test results, Compritol 888 ATO (as the solid lipid), MCT oil (as the liquid lipid), and Tween 80 (as the surfactant) were were chosen for the formulation of the desired NLCs. Compritol 888 ATO is recognized as a highly valued ingredients for preparing NLC/SLN formulations due to its low cytotoxicity (44). It is effective in enhancing drug entrapment efficiency and facilitating the delivery of both hydrophilic and lipophilic drug (44). MCT oil, characterized by its shorter carbon chain, offers improved drug loading capacity and accelerates release rates (45). Tween 80 serves as a non-ionic surfactant that ensures a stable and consistent lipid dispersion in the aqueous phase, promoting effective drug release from the lipid matrix (46). Additionally, raising their concentration in formulations may lead to a reduction in particle size by decreasing the surface rigidity between the aqueous medium and the lipid. The increasing ratio of liquid lipids to solid lipids lowers the possibility of nanoparticle aggregation despite the increase in their particle size (47). The solid-to-liquid lipids were used in a ratio of 70:30 (48).

The formulation F6, containing 5 mg mL^{-1} Co-Q10 and 5 mg mL^{-1} LE (highest level of ingredients), was selected for TEM analysis, along with F2 (containing 5 mg mL^{-1} Co-Q10), F3 (containing 5 mg mL^{-1} LE) were selected for thermal analysis (DSC) and FT-IR evaluation. All prepared formulations were utilized to

investigate the combined effects of Co-Q10 and LE on ROS levels, melanin content, and antityrosinase activity.

Physicochemical characterization of the Co-Q10/LE-NLCs

Particle size is a serious surface property for nanocarriers, significantly impacting stability, *EE* %, drug release, and biodistribution (49). Studies have indicated that lipid-based nanocarriers with a Z-average diameter of 600 nm or greater are unable to transport encapsulated active substances into the lower layers of the stratum corneum (49). Nanocarriers with a Z-average diameter of 300 nm or less are capable of transporting their active ingredients into the deeper skin layers (50). The Z-average size measurements for freshly prepared NLC suspensions are presented in Table I. The Z-average size for the NLC formulations was observed to be less than 248 nm and ranged from 146 to 248 nm. In addition, the particle size increased in formulations containing a higher ratio of LE to Co-Q10.

The polydispersity index reflects the range of particle sizes within a given sample. PDI values range from 0.0, indicating a uniform particle size, to 1.0, which signifies a sample with a wide variety of particle sizes (49). A PDI value of less than 0.2 is typically associated with enhanced long-term stability of NLC formulations (51). The formulations F1 to F8 displayed PDI values that were relatively low, falling between 0.21 and 0.27.

Zeta potential indicates the surface charge, physical stability, and binding affinity with surrounding ions (51). All NLC formulations exhibited a zeta potential ranging from −5 to −15 mV. In formulations with different Co-Q10/LE ratios, the zeta potential was lower than blank (drug-free) NLC.

Table I. The surface characteristics and the percentage of the components of Co-Q10/ LE-loaded NLC (equivalent amounts in moles and µg mL^{-1}, refer to Table S3 in the supplementary file)

Formulation	Compritol (%)	MCT Oil (%)	Tween 80 (%)	Co-Q10 (%)	LE (%)	Z-Average (nm) ± SD	PDI ± SD	Zeta Potential (mV) ± SD	Colour
F1	3.5	1.5	5	–	–	244.5 ± 3.34	0.259 ± 0.003	–5.00 ± 0.70	White
F2				0.50	–	201.5 ± 1.08	0.222 ± 0.004	–12.70 ± 2.36	Yellow
F3				–	0.50	241.7 ± 4.50	0.230 ± 0.008	–14.71 ± 1.03	Light brown
F4				0.25	–	155.7 ± 5.11	0.166 ± 0.010	–10.80 ± 1.78	Yellow
F5				–	0.25	226.5 ± 2.31	0.278 ± 0.012	–6.92 ± 1.89	Light brown
F6				0.50	0.50	162.7 ± 2.19	0.273 ± 0.001	–13.20 ± 1.59	Mustard yellow
F7				0.50	0.25	146.3 ± 3.42	0.210 ± 0.007	–15.75 ± 1.02	Mustard yellow
F8				0.25	0.50	248.1 ± 1.08	0.279 ± 0.004	–10.70 ± 2.36	Mustard yellow

TEM measurement

The microscopic morphology for F6 is shown in Fig. 2. The surface modification results using TEM revealed a rounded shape and excellent dispersibility of nano-sized particles. The mean size of the selected Co-Q10/LE-NLC was about 100 nm.

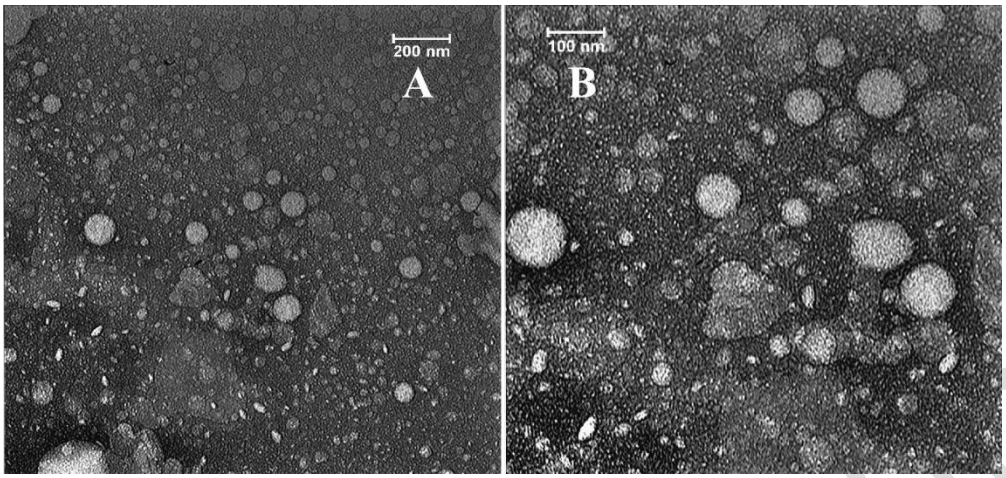

Fig. 2. TEM image of Co-Q10/LE-NLC (F6). Scale bar: a) 200 nm; b) 100 nm.

Differential scanning calorimetry (DSC)

The DSC analyzer is widely recognized for assessing the melting and recrystallization characteristics of NLC (52). Evaluating the extent of lipid crystallization and modification is crucial for determining the quality and stability of NLC/SLN formulations (53). The melting peaks of Co-Q10 and Compritol were obtained at 51 and 70 °C, respectively, which was consistent with their expected melting temperatures (Fig. 3a). The melting point of Compritol decreased from 73 ˚C to 65 °C for NLC formulations attributed to the imperfection within the lipid structure introduced by the NLC system. In formulations containing Co-Q10, the peak at 51 °C belonging to Co-Q10 disappeared. This phenomenon is consistent with previous studies showing that encapsulation in lipid matrices alters the crystalline structure of Co-Q10 (28). The enthalpy value was another indicator of the crystal order (52). Higher melting enthalpy values indicate a higher-ordered network arrangement and vice versa. The enthalpy value of Compritol was significantly greater than the value for drug-free lyophilized NLC (112.03 J g^{-1} in the lipid bulk compared to 51.41 J g^{-1} in the drug-free lyophilized NLC), suggesting a disruption in crystal structure within the NLC formulations (54).

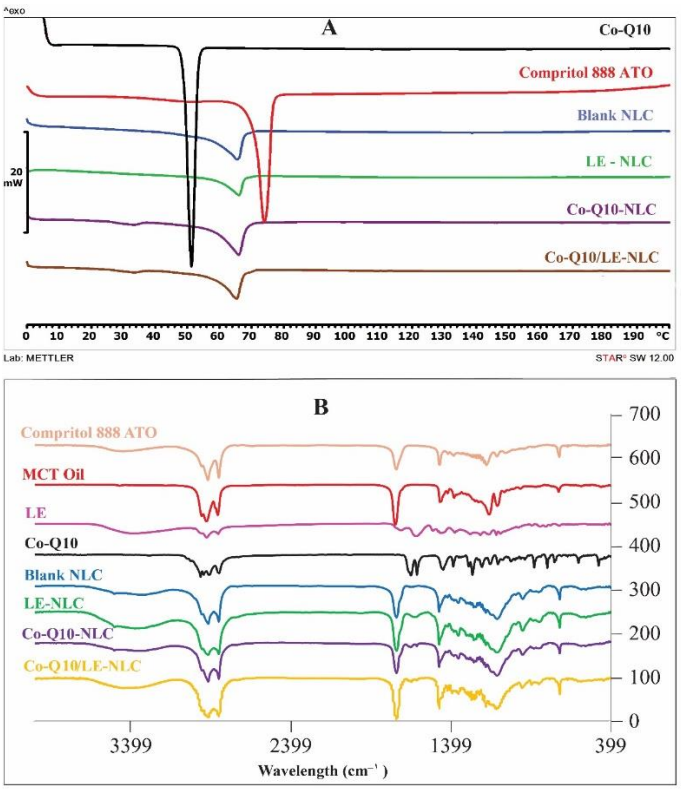

Fig. 3. a) DSC curves of Co-Q10, solid lipid, freeze-dried blank NLC (F1) and Co-Q10/LE-loaded NLC (F2, F3, and F6); b) The FT-IR spectra of Co-Q10, LE, freeze-dried blank NLC (F1), and Co-Q10/LE-NLCs (F2, F3, and F6), and at 4000–400 cm^{-1} range.

Fourier transform infrared (FT-IR) spectra

The infrared spectra of lipids, LE, Co-Q10, and NLC formulations F1, F2, F3, and F6 were analyzed within the 400–4000 cm^{-1} range (Fig. 3b and Fig S1 in supplementary file):

- Lipid matrix characterization: Compritol and MCT oil showed carbonyl stretching vibrations at 1739 cm^{-1} and 1745 cm^{-1}, respectively, consistent with the literature on saturated triglycerides. No peak shifts were observed in NLC formulations, indicating lipid matrices (55).
- Co-Q10 and LE structural integrity: The Co-Q10 characteristic peaks at 1648 cm^{-1} (C=O stretching) and 1610 cm^{-1} (C=C stretching) were presented in F2 and F6 spectra. Similar retention of carbonyl signatures was reported in FT-IR studies of lipid-encapsulated bioactive compounds, confirming structural stability during nanoparticle synthesis (55). LE's hydroxyl (3378.6 cm^{-1}) and flavonoid-associated C=O (1710.3 cm^{-1})/C=C (1618 cm^{-1}) vibrations remained unaltered in F3 and F6. This matches observations in plan extract encapsulation studies, where FT-IR verifies flavonoid integrity post-encapsulation (36).

Moreover, no new peaks were detected in NLC formulations containing Co-Q10 and LE, suggesting no chemical reaction occurred. Therefore, considering the FT-IR spectrum for F1 (blank NLC), F2 (Co-Q10-NLC), F3 (LE-NLC), and F6, the analysis suggests that the active components were exclusively encapsulated within the lipid matrix (55).

Entrapment efficiency (EE) %

The log*P* value quantifies a compound's distribution between organic and aqueous phases, indicating its lipophilicity or hydrophilicity (56). Higher log*P* values suggest greater affinity for lipophilic environments, while lower values indicate a preference for aqueous environments. This parameter is vital in drug development, influencing pharmacokinetic properties such as absorption, distribution, metabolism, and excretion (ADME) (56). Given the substantial lipophilicity of Co-Q10 (log*P* > 10), its dissolution and stability in an aqueous medium are critical. Therefore, the detectable concentration of Co-Q10 in the media passed through the filter (using an indirect method) fell below the LOQ. Therefore, the *EE* % of Co-Q10 was measured using the direct method. Also, considering the LOQ, the amount of liquiritin and glabridin was determined using indirect and direct methods, respectively. The *EE* % of fresh NLC systems F2, F3, and F6 was reported in Table II. High encapsulation of Co-Q10 was observed in formulations F2 and F6, with F2 demonstrating higher encapsulation level. Specifically, F2 contained 5 mg mL^{-1} of Co-Q10, whereas F6 included 5 mg of Co-Q10 mL^{-1} alongside with 5 mg mL^{-1} LE. Additionally, the loading amounts for liquiritin and glabridin in formulation F3 were greater than those in F6. Formulation F7 (5 mg mL^{-1} Co-Q10 + 2.5 mg mL^{-1} LE) showed slightly higher Co-Q10 entrapment than F6, while F8 (2.5 mg mL^{-1} Co-Q10 + 5 mg mL^{-1} LE) showed a slightly higher glabridin *EE* % than F6 and F7. The liquiritin entrapment efficiency decreased slightly in F7 but remained comparable between F6 and F8.

The *EE* % was re-evaluated for formulations F2, F3, and F6 after a period of six months. The findings revealed only a minor reduction in the *EE* % of these formulations, suggesting that they maintained chemical stability over time (Table II). This supports the conclusion that NLC serves as a suitable nanocarrier for the incorporation Co-Q10 and LE, enhancing their chemical stability (57).

Table II. The encapsulation efficiency (EE %) of NLC formulations F2, F3, F6, F7, and F8 was determined both immediately after preparation and after 6 months of storage

Formulation	*EE* %					
	Fresh			After 6 months		
	Co-Q10	Liquiritin	Glabridin	Co-Q10	Liquiritin	Glabridin
F2	87.21 ± 1.42	–	–	82.45 ± 2.4	–	–
F3	–	66.78 ± 3.12	73.25 ± 2.57	–	59.52 ± 4.12	68.56 ± 3.59
F6	76.56 ± 2.42	60.21 ± 2.97	69.57 ± 1.68	74.75 ± 4.21	58.18 ± 3.22	63.52 ± 4.09
F7	79.28 ± 3.75	58.46 ± 2.63	68.05 ± 3.42	–	–	–
F8	78.60 ± 2.75	60.37 ± 4.21	71.97 ± 2.48	–	–	–

Physiochemical stability

The surface characteristics of blank NLC and Co-Q10/LE-NLC (F1-F8) formulations were investigated for stability over time. Measurements of particle size, PDI, and zeta potential for the F1-F8 were taken after 1, 3, and 6 months at various temperatures (Table III). In addition, there was no apparent evidence of instability, like color changes or phase separation, and no notable alterations in the Z-average size and PDI. Zeta potential measurements were conducted for all formulations over a period of six months, with the exception of F3, which exhibited instability after three months.

Table III. Physiochemical stability of Co-Q10/LE-NLCs over time and temperature

Code	Temp. (° C)	Time (month)	Z-average size (nm) ± SD	PDI ± SD	Zeta potential (mV) ± SD	Homogeneity/ color
F1		0	244.5 ± 3.34	0.259 ± 0.003	–5.0 ± 0.70	Homogenous/ white
	4	1	242.3 ± 4.23	0.329 ± 0.002	–7.5 ± 0.23	Homogenous/ white
		3	251.4 ± 0.89	0.331 ± 0.009	–7.1 ± 0.22	Homogenous/ white
		6	278.3 ± 2.45	0.346 ± 0.008	–6.2 ± 0.31	Homogenous/ white
	25	1	217.4 ± 1.56	0.463 ± 0.003	–6.7 ± 0.31	Homogenous/ white
		3	192.2 ± 1.23	0.512 ± 0.013	–6.0 ± 0.24	Homogenous/ white
		6	208.2 ± 2.315	0.586 ± 0.018	–5.8 ± 0.34	Homogenous/ white
	40	1	248.8 ± 1.59	0.479 ± 0.003	–3.39 ± 0.40	Homogenous/ white
		3	237.2 ± 1.37	0.461 ± 0.009	–3.86 ± 0.24	Homogenous/ white
		6	249.4 ± 2.24	0.481 ± 0.007	–3.12 ± 0.22	Homogenous/ white
F2		0	201.5 ± 1.08	0.222 ± 0.004	–12.70 ± 2.36	Homogenous/ yellow
	4	1	209.7 ± 2.95	0.263 ± 0.012	–19.7 ± 0.09	Homogenous/ yellow
		3	207.2 ± 1.87	0.245 ± 0.017	–16.7 ± 0.24	Homogenous/ yellow
		6	221.3 ± 2.5	0.289 ± 0.008	–15.8 ± 0.17	Homogenous/ yellow
	25	1	211.3 ± 1.86	0.25 ± 0.003	–13.0 ± 0.19	Homogenous/ yellow
		3	220.0 ± 1.75	0.262 ± 0.017	–13.6 ± 0.24	Homogenous/ yellow
		6	234.1 ± 3.18	0.275 ± 0.024	–16.7 ± 0.25	Homogenous/ yellow
	40	1	208.8 ± 1.95	0.285 ± 0.008	–12.9 ± 0.38	Homogenous/ yellow
		3	187.3 ± 1.02	0.253 ± 0.026	–7.48 ± 0.18	Homogenous/ yellow
		6	213.2 ± 1.89	0.245 ± 0.008	–11.2 ± 0.24	Homogenous/ yellow
F3		0	241.7 ± 4.50	0.230 ± 0.008	–14.71 ± 1.03	Homogenous/ light brown
	4	1	286.2 ± 2.95	0.299 ± 0.012	–17.5 ± 0.09	Homogenous/ light brown
		3	294.3 ± 2.12	0.298 ± 0.015	–16.0 ± 0.15	Homogenous/ light brown
		6	325.1 ± 3.7	0.301 ± 0.008	–17.2 ± 0.24	Homogenous/ light brown
	25	1	270.6 ± 1.86	0.303 ± 0.003	–12.4 ± 0.19	Homogenous/ light brown

		3	446.4 ± 1.75	0.310 ± 0.017	–12.5 ± 0.24	Homogenous/ light brown
		6	–	–	–	Sediment formation/ light brown
	40	1	251.6 ± 1.95	0.29 ± 0.008	–12.7 ± 0.38	Homogenous/ light brown
		3	324.5 ± 1.02	0.267 ± 0.026	–9.6 ± 0.18	Homogenous/ light brown
		6	–	–	–	Sediment formation / light brown
F4		0	155.7 ± 5.11	0.166 ± 0.010	–10.80 ± 1.78	Homogenous/ yellow
	4	1	154.1 ± 0.76	0.168 ± 0.003	–10.87 ± 1.33	Homogenous/ yellow
		3	155.5 ± 2.40	0.173 ± 0.006	–11.21 ± 0.98	Homogenous/ yellow
		6	158.1 ± 3.27	0.175± 0.004	–11.05 ± 1.03	Homogenous/ yellow
	25	1	159.7 ± 2.34	0.176 ± 0.005	–11.71 ± 1.34	Homogenous/ yellow
		3	158.8 ± 1.62	0.214 ± 0.006	–9.83 ± 0.38	Homogenous/ yellow
		6	164.9 ± 2.49	0.279 ± 0.009	–9.30 ± 1.08	Homogenous/ yellow
	40	1	159.2 ± 1.45	0.174 ± 0.007	–10.21 ± 0.78	Homogenous/ yellow
		3	162.3 ± 1.42	0.214 ± 0.008	–9.62 ± 1.74	Homogenous/ yellow
		6	166.4 ± 2.89	0.226 ± 0.008	–8.74 ± 1.32	Homogenous/ yellow
F5		0	226.5 ± 2.31	0.278 ± 0.012	–6.92 ± 1.89	Homogenous/ light brown
	4	1	235.2 ± 2.16	0.272 ± 0.013	–7.42 ± 0.79	Homogenous/ light brown
		3	287.4 ± 1.42	0.283 ± 0.007	–6.47 ± 1.25	Homogenous/ light brown
		6	295.1 ± 3.35	0.308 ± 0.019	–7.21 ± 1.65	Homogenous/ light brown
	25	1	279.5 ± 3.12	0.293 ± 0.006	–6.91 ± 0.78	Homogenous/ light brown
		3	338.3 ± 2.74	0.310 ± 0.015	–6.82 ± 1.13	Homogenous/ light brown
		6	423.4 ± 1.36	0.354 ± 0.006	–5.43 ± 1.46	Homogenous/ light brown
	40	1	269.3 ± 1.79	0.302 ± 0.008	–7.68 ± 0.89	Homogenous/ light brown
		3	316.6 ± 2.32	0.267 ± 0.015	–9.6 ± 0.18	Homogenous/ light brown

		6	–	–	–	Sediment formation/ light brown
F6		0	162.7 ± 2.19	0.273 ± 0.001	–13.2 ± 1.59	Homogenous/ mustard yellow
	4	1	165.3 ± 2.95	0.301 ± 0.012	–17.6 ± 0.09	Homogenous/ mustard yellow
		3	172.3 ± 1.64	0.321 ± 0.021	–14.6 ± 0.48	Homogenous/ mustard yellow
		6	175.1 ± 4.01	0.357 ± 0.007	–14.9 ± 0.36	Homogenous/ mustard yellow
	25	1	169.6 ± 1.75	0.297 ± 0.004	–10.4 ± 0.26	Homogenous/ mustard yellow
		3	166.2 ± 1.75	0.303 ± 0.017	-6.2 ± 0.24	Homogenous/ mustard yellow
		6	175.3 ± 2.56	0.351 ± 0.024	–7.7 ± 0.31	Homogenous/ mustard yellow
	40	1	141.6 ± 1.78	0.287 ± 0.009	–8.6 ± 0.27	Homogenous/ mustard yellow
		3	182.7 ± 1.02	0.282 ± 0.026	-6.8 ± 0.18	Homogenous/ mustard yellow
		6	203.1 ± 2.36	0.297 ± 0.007	-6.3 ± 0.24	Homogenous/ mustard yellow
F7		0	146.3 ± 3.42	0.21 ± 0.007	–15.75 ± 1.02	Homogenous/ mustard yellow
	4	1	138.9 ± 2.95	0.213 ± 0.012	–17.6 ± 0.09	Homogenous/ mustard yellow
		3	148.1 ± 2.31	0.228 ± 0.026	–16.8 ± 0.21	Homogenous/ mustard yellow
		6	153.1 ± 3.21	0.251 ± 0.008	–16.1 ± 0.37	Homogenous/ mustard yellow
	25	1	154.2 ± 1.86	0.243 ± 0.003	–11.0 ± 0.19	Homogenous/ mustard yellow
		3	145.6 ± 1.75	0.232 ± 0.017	–14.5 ± 0.24	Homogenous/ mustard yellow
		6	152.4 ± 2.38	0.253 ± 0.022	–14.6 ± 0.37	Homogenous/ mustard yellow
	40	1	141.7 ± 2.23	0.257 ± 0.007	–9.8 ± 0.41	Homogenous/ mustard yellow
		3	147.4 ± 1.02	0.210 ± 0.026	–10.1 ± 0.18	Homogenous/ mustard yellow
		6	150.3 ± 2.51	0.245 ± 0.018	–9.8 ± 0.23	Homogenous/ mustard yellow
F8		0	248.1 ± 1.08	0.279 ± 0.004	–10.7 ± 2.36	Homogenous/ mustard yellow
	4	1	291.8 ± 2.95	0.313 ± 0.012	–14.8 ± 0.09	Homogenous/ mustard yellow
		3	304.4 ± 1.75	0.321 ± 0.024	–14.1 ± 0.17	Homogenous/ mustard yellow
		6	321.1 ± 3.74	0.350 ± 0.007	–9.7 ± 0.24	Homogenous/ mustard yellow

25	1	257.2 ± 1.86	0.287 ± 0.003	–10.7 ± 0.19	Homogenous/ mustard yellow
	3	257.9 ± 1.75	0.330 ± 0.017	–8.7 ± 0.24	Homogenous/ mustard yellow
	6	261.2 ± 2.54	0.381 ± 0.018	–7.9 ± 0.32	Homogenous/ mustard yellow
40	1	237.3 ± 1.95	0.312 ± 0.008	–13.4 ± 0.38	Homogenous/ mustard yellow
	3	298.1 ± 1.02	0.286 ± 0.026	-6.6 ± 0.18	Homogenous/ mustard yellow
	6	324.7 ± 2.54	0.324 ± 0.012	-6.6 ± 0.51	Homogenous/ mustard yellow

Cell viability

The cytotoxicity effect of the NLC formulations (F1-F8) at a dosage of 1 % (*V/V*) following a 24-hour incubation was investigated using an MTT assay (Fig. 4a). Results confirm no significant difference in B16F10 cell viability treated with 1 % NLCs when evaluated against the control group. Also, the protective effect of NLCs containing Co-Q10, LE, and the combination of both against H_2O_2 was evaluated (Fig. 4b). Results confirmed that cell treatment with H_2O_2-induced cytotoxicity after 90 min, while pretreatment with NLC formulations could partially protect against H_2O_2 toxicity. Formulations F6, F7 and F8, containing a combination of Co-Q10 and LE, demonstrated enhanced cytoprotective properties against oxidative damage in B16F10 cells.

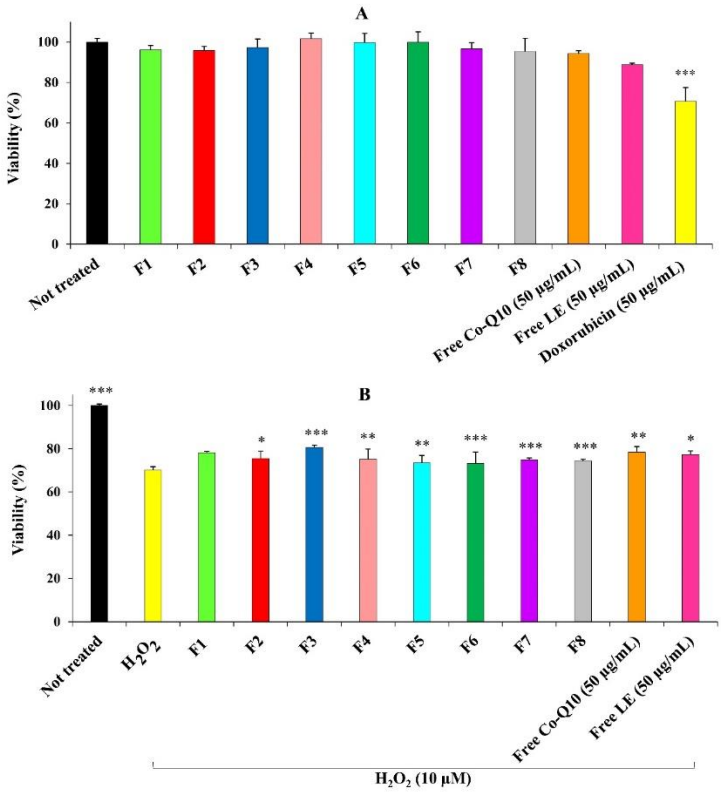

Fig. 4. a) Cytotoxicity and b) cytoprotective effects of NLC formulations (at 1 % concentration in cell culture media) in the MTT assay. Results are presented as mean ± SEM (n = 3). Asterisks indicate

statistically significant differences compared to the non-treated (a) and H_2O_2 (b) groups: *$p < 0.05$, **$p < 0.01$, ***$p < 0.001$.

Cellular ROS level determination

Oxidative stress occurs when there is a disruption between the generation of ROS and the body's antioxidant defenses (58). H_2O_2 application is a commonly used method for the expression of oxidative damage/stress in cell models (58). Coenzyme Q10, as an electron transport agent, is capable of suppressing intracellular ROS (59). Within cells, the benzoquinone structure of Coenzyme Q10 can exist in three interconvertible oxidation states: the reduced form ubiquinol (Co-Q10H_2), the ubisemiquinone intermediate (Co-Q10H$^{\bullet}$), and the fully oxidized ubiquinone (Co-Q10). This redox state is supported by additional antioxidant sources, like α-tocopherol and vitamin C (60). The synergistic effects of Co-Q10 in combination with other antioxidants, such as beta-carotene (61) and astaxanthin (62), have been reported previously. Co-Q10 and licorice extracts, as antioxidants, can reduce cellular imbalance caused by increased ROS levels (59). They were encapsulated in NLC as lipophilic ingredients to improve their distribution in an aqueous medium (63). We applied 10 mmol L^{-1} H_2O_2 for 90 minutes, which led to approximately 70 % cell viability.

The effective dose (ED50) refers to the amount of a drug required to produce a specified biological response in 50 % of the population, serving as a benchmark for assessing the drug's effectiveness (64, 65). The ED50 values for both active ingredients underwent isobolographic analysis to evaluate the nature of their interaction when Co-Q10 and LE were administered together (64, 65). The interaction index is derived from the ED50 values of the individual components in relation to their combined effects. An interaction index greater than 1 indicates antagonism, an index of 1 signifies an additive effect (no interaction), and an index less than 1 suggests synergism (65, 66).

Coenzyme Q10 was entrapped in three constant ratios with LE in NLC nanocarriers, and we investigated its synergistic effect in suppressing ROS. The effect of NLC formulations on scavenging the ROS was investigated in 0, 12, 25, and 50 µmol L^{-1} of active ingredient at 1:1, 1:0.5, and 0.5:1 constant ratios. The DCF absorbance results (Fig. 5) revealed that intracellular ROS levels rose following treatment with H_2O_2 compared to the negative control group. Pretreatment with Co-Q10/LE-NLCs decreased ROS production in a concentration-dependent manner. Cell pretreatment with blank NLC at a concentration of 1 % showed no significant effect on ROS production. All NLC formulations, including a combination of Co-Q10/LE, were more capable of ROS scavenging than NLCs loaded with a single ingredient. According to the CalcuSyn analysis, the interaction index values for F6, F7, and F8 were 1.0, 0.9, and 0.6, respectively (Table IV). Therefore, the F6 containing an equal amount of Co-Q10 and LE had an additive effect on inhibiting ROS production. The F7 containing Co-Q10/LE at a ratio of 1/0.5 exerted a synergistic effect. Also, a stronger synergistic effect was observed for F8, which contains a 0.5:1 ratio of Co-Q10/LE. Due to its high content of flavonoids, LE is an effective antioxidant and anti-inflammatory agent (67).

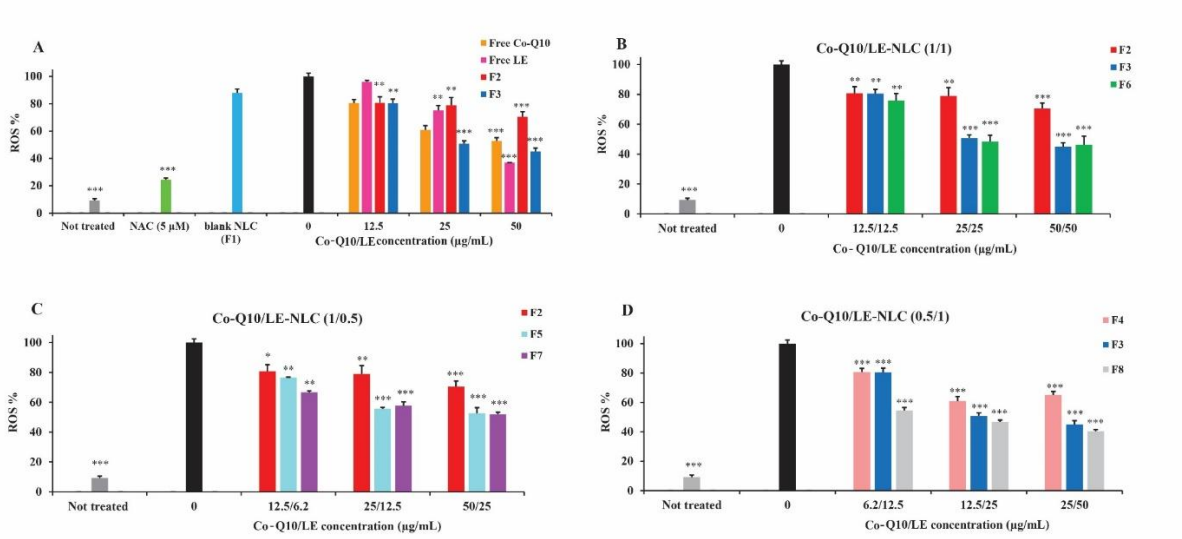

Fig. 5. Enhanced ROS Production in the Presence of LE/Q10-NLC. A: Effect of free vs encapsulated single Co-Q10 and LE. NAC (N-acetylcysteine) is a positive control. B: Effect of 1:1 ratio Co-Q10/LE formulation vs single ingredient formulations. C: Effect of 1:0.5 ratio. D. Effect of 0.5:1 ratio. Results are expressed as mean ± SEM (n = 3). Asterisks denote statistical significance compared to control (H_2O_2 treatment only): *$p < 0.05$, **$p < 0.01$, ***$p < 0.001$.

Table IV. ED50 and interaction index values for F6, F7, and F8 in ROS, tyrosinase, and melanin levels

Formulation	Co-Q10/LE ratio	ROS Inhibition		Antityrosinase activity		Melanin synthesis inhibition	
		Interaction index values	ED50 values (μg mL^{-1})	Interaction index values	ED50 values (μg mL^{-1})	Interaction index values	ED50 values (μg mL^{-1})
F6	1:1	1.02	40.86 ± 0.16	0.78	167.04 ± 0.53	2.46	45.03 ± 0.26
F7	1:0.5	0.98	49.44 ± 0.22	0.56	358.08 ± 1.61	0.70	41.36 ± 0.41
F8	0.5:1	0.62	21.72 ± 0.19	0.48	101.33 ± 0.62	1.78	27.34 ± 0.15

Melanin production study

The melanin level graphs (Fig. 6 and Fig. 1S in supplementary data) indicate that melanin production was reduced in the melanoma cells treated with Co-Q10/LE-NCLs relative to the untreated cells, those treated with blank NCL, free Co-Q10 or free LE and kojic acid (positive control). The effect of NLCs containing Co-Q10 and LE on melanin content was consistent with the tyrosinase-inhibitory activity.

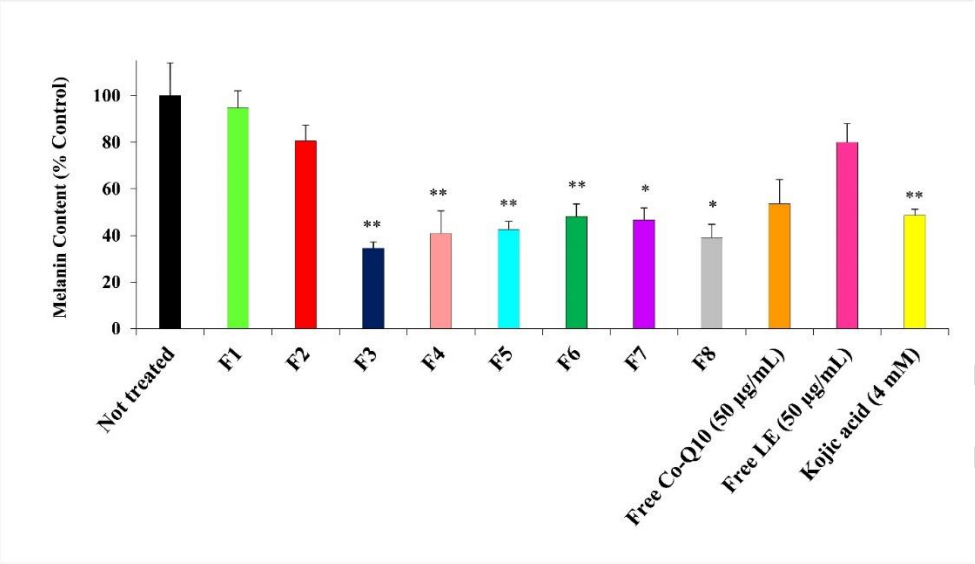

Fig. 6. Effect of Q10/LE-NLC formulations 1/1, 1/0.5, 0.5/1 on melanin content in B16F10 cells after 24 hours. Results are mean ± SEM (n = 3). The asterisks indicate statistical differences obtained compared to not treated group shown in the figure as *p < 0.05, **p < 0.01, and ***p < 0.001.

Cellular tyrosinase activity assay

DOPA assay is a spectrophotometric assay indicating tyrosinase activity (63). Recently, Co-Q10 was found to be an inhibitor of tyrosinase activity (68). Co-Q10 downregulates melanin synthesis by suppressing MITF-expressing and cAMP-mediated CREB signaling cascades (68). Liquiritin and glabridin are promising depigmenting agent compounds in licorice extract. The synergistic effect of Co-Q10 and glabridin on tyrosinase activity has been reported previously (60). Co-Q10 and LE are natural tyrosinase inhibitors that have no side effects, like dermatitis, compared to other inhibitors of melanin synthesis, like arbutin, kojic acid, hydroquinone, corticosteroids, and mercury (60).

We evaluated the synergistic effect of encapsulated NLC of Co-Q10 and LE in 1/1, 0.5/1, and 1/0.5 ratios on tyrosinase activity in B16F10 cells (Fig. 7 and 2S in supplementary file). The tyrosinase activity in these cells, following administration of both blank and Co-Q10/LE-loaded NLC formulations, was compared to their respective control groups, as shown in Fig. 7. Both free Co-Q10 and the Co-Q10-NLC (F4) did not demonstrate any significant impact on tyrosinase enzyme activity, similar to the blank NLC. The interaction index values for F6, F7, and F8 were calculated as 0.78, 0.56, and 0.48, respectively (Table IV). All NLC formulations containing a combination of Co-Q10 and LE showed a synergistic inhibitory effect on tyrosinase activity, similar to the ROS-inhibitory effect. The order was: F8 (Co-Q10/LE: 1/1) > F7 (Co-Q10/LE: 1/0.5) > F6 (Co-Q10/LE: 0.5/1).

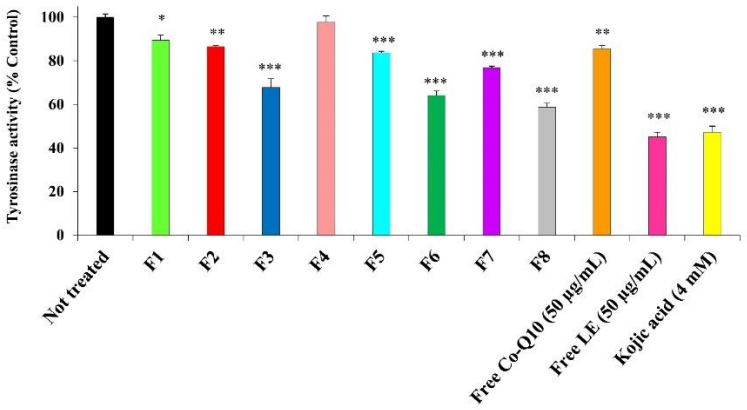

Fig. 7. Effect of Q10/LE-NLC formulations 1/1, 1/0.5, 0.5/1 on tyrosinase activity in B16F10 cells after 24 h. Results are mean ± SEM (n = 3). The asterisks indicate statistical differences obtained compared to not treated group *p < 0.05, **p < 0.01, and ***p < 0.001.

CONCLUSIONS

We developed novel NLC formulations containing Co-Q10 and LE, both individually and in combination, to improve the efficacy of natural products. In conclusion, all NLCs demonstrated favorable surface properties, good physicochemical stability, including particle sizes ranging from 146 to 248 nm, polydispersity indices (PDI) between 0.21 and 0.27, and zeta potentials from –5 to –15 mV, indicating good physicochemical stability. The *EE* % for active ingredients was consistently above 60 %. Our formulations demonstrated robust stability over six months. Key parameters like particle size, polydispersity index (PDI), and zeta potential remained stable under various storage conditions. No visible signs of degradation, such as phase separation or color changes, were detected. Although minor decreases in entrapment efficiency (*EE* %) were observed in some formulations (F2, F3, and F6), the NLC system effectively preserved the stability of Co-Q10 and LE over time. The synergistic antioxidant and antityrosinase activity of Co-Q10-NLC, LE-NLC, and Co-Q10/LE-NLC confirmed that F8 (Co-Q10/LE: 0.5/1 loaded NLC) showed the strongest synergistic effect on ROS suppression and tyrosinase inhibition. F7 (Co-Q10/LE: 1/0.5 loaded NLC) also exerted a synergistic effect in both experiments. F6 (Co-Q10/LE: 1/1 loaded NLC) had an additive effect on ROS scavenging and a synergistic effect on decreasing tyrosinase activity. Therefore, a combination of Co-Q10/LE-loaded NLC at a 0.5/1 ratio is recommended as a topical agent for antiaging and skin-lightening. Future research will involve *in vivo* trials to validate the formulations' safety and efficacy in clinical settings. Additionally, optimizing these formulations for large-scale production and exploring other bioactive compounds within the NLC framework could expand their potential in dermatology and cosmetics.

Acknowledgments. – The research was supported by Mashhad University of Medical Sciences (grant number 4021191).

Conflict of interest. – The authors declare no conflict of interest.

Authors contributions. – Hoda Atapour-Mashhad: Conceptualization, Methodology, Investigation, Data curation, Writing - original draft.

Afsaneh Hoseinsalari: Conceptualization, Investigation, Formal analysis, Writing - review & editing.
Zahra Tayarani-Najaran: Supervision, Writing - review & editing.
Javad Asili: Methodology, Resources.
Armita Sedighidarijani: Writing - review & editing.
Shiva Golmohammadzadeh: Conceptualization, Project administration, Supervision.

REFERENCES

1. Hussein RS, Bin Dayel S, Abahussein O, El-Sherbiny AA, Influences on Skin and Intrinsic Aging: Biological, Environmental, and Therapeutic Insights, *J Cosmet Dermatol* **24**(2) (2025) e16688; https://doi.org/10.1111/jocd.16688
2. Bang E, Kim DH, Chung HY, Protease-activated receptor 2 induces ROS-mediated inflammation through Akt-mediated NF-κB and FoxO6 modulation during skin photoaging, *Redox Biol* **44** (2021) 102022; https://doi.org/10.1016/j.redox.2021.102022
3. Papaccio F, A DA, Caputo S, Bellei B, Focus on the Contribution of Oxidative Stress in Skin Aging, *Antioxidants (Basel)* **11**(6) (2022) 1121; https://doi.org/10.3390/antiox11061121
4. Rinnerthaler M, Bischof J, Streubel MK, Trost A, Richter K, Oxidative stress in aging human skin, *Biomolecules* **5**(2) (2015) 545–589; https://doi.org/10.3390/biom5020545
5. Dall'Olmo L, Papa N, Surdo NC, Marigo I, Mocellin S, Alpha-melanocyte stimulating hormone (α-MSH): biology, clinical relevance and implication in melanoma, *J Transl Med* **21**(1) (2023) 562; https://doi.org/10.1186/s12967-023-04405-y
6. Netcharoensirisuk P, Umehara K, De-Eknamkul W, Chaotham C, Cajanin Suppresses Melanin Synthesis through Modulating MITF in Human Melanin-Producing Cells, *Molecules* **26**(19) (2021) 6040; https://doi.org/10.3390/molecules26196040
7. Solano F, Photoprotection and Skin Pigmentation: Melanin-Related Molecules and Some Other New Agents Obtained from Natural Sources, *Molecules* **25**(7) (2020) 1537; https://doi.org/10.3390/molecules25071537
8. Du D, Su Y, Shang Q, Chen C, Tang W, Zhang L, et al, Biomimetic synthesis of L-DOPA inspired by tyrosine hydroxylase, *J Inorg Biochem* **234** (2022) 111878; https://doi.org/10.1016/j.jinorgbio.2022.111878
9. Song H, Hwang YJ, Ha JW, Boo YC, Screening of an epigenetic drug library identifies 4-((hydroxyamino) carbonyl)-N-(2-hydroxyethyl)-N-phenyl-benzeneacetamide that reduces melanin synthesis by inhibiting tyrosinase activity independently of epigenetic mechanisms, *Int J Mol Sci* **21**(13) (2020) 4589; https://doi.org/10.3390/ijms21134589
10. Ferreira KCB, Valle A, Paes CQ, Tavares GD, Pittella F, Nanostructured Lipid Carriers for the Formulation of Topical Anti-Inflammatory Nanomedicines Based on Natural Substances, *Pharmaceutics* **13**(9) (2021) 1454; https://doi.org/10.3390/pharmaceutics13091454
11. Noh YH, Kim KY, Shim MS, Choi SH, Choi S, Ellisman MH, et al, Inhibition of oxidative stress by coenzyme Q10 increases mitochondrial mass and improves bioenergetic function in optic nerve head astrocytes, *Cell Death Dis* **4**(10) (2013) e820; https://doi.org/10.1038/cddis.2013.341
12. Li L, Du J, Lian Y, Zhang Y, Li X, Liu Y, et al, Protective effects of coenzyme Q10 against hydrogen peroxide-induced oxidative stress in PC12 cell: the role of Nrf2 and antioxidant enzymes, *Cell Mol Neurobiol* **36** (2016) 103–111; https://doi.org/10.1007/s10571-015-0224-4

13. Hernández-Camacho JD, Bernier M, López-Lluch G, Navas P, Coenzyme Q(10) Supplementation in Aging and Disease, *Front Physiol* **9** (2018) 44; https://doi.org/10.3389/fphys.2018.00044
14. Rosita N, Meitasari VA, Rianti MC, Hariyadi DM, Miatmoko A, Enhancing skin penetration of epigallocatechin gallate by modifying partition coefficient using reverse micelle method, *Ther Deliv* **10**(7) (2019) 409-417; https://doi.org/10.4155/tde-2019-0015
15. Ayunin Q, Miatmoko A, Soeratri W, Erawati T, Susanto J, Legowo D, Improving the anti-ageing activity of coenzyme Q10 through protransfersome-loaded emulgel, *Sci Rep* **12**(1) (2022) 906; https://doi.org/10.1038/s41598-021-04708-4
16. Sharma V, Katiyar A, Agrawal R, *Glycyrrhiza glabra*: chemistry and pharmacological activity, *Sweeteners* **31** (2017) 87–100; https://doi.org/10.1007/978-3-319-27027-2_21
17. Wahab S, Annadurai S, Abullais SS, Das G, Ahmad W, Ahmad MF, et al, *Glycyrrhiza glabra* (Licorice): A Comprehensive Review on Its Phytochemistry, Biological Activities, Clinical Evidence and Toxicology, *Plants (Basel)* **10**(12) (2021) 2751; https://doi.org/10.3390/plants10122751
18. Xing M, Wang X, Zhao L, Zhou Z, Liu H, Wang B, et al, Novel dissolving microneedles preparation for synergistic melasma therapy: Combined effects of tranexamic acid and licorice extract, *Int J Pharm* **600** (2021) 120406; https://doi.org/10.1016/j.ijpharm.2021.120406
19. Tian M, Yan H, Row KH, Simultaneous extraction and separation of liquiritin, glycyrrhizic acid, and glabridin from licorice root with analytical and preparative chromatography, *Biotechnol Bioprocess Eng* **13**(6) (2008) 671-676; https://doi.org/10.1007/s12257-008-0019-2
20. Draelos ZD, Skin lightening preparations and the hydroquinone controversy, *Dermatol. Ther.* **20**(5) (2007) 308-313; https://doi.org/10.1111/j.1529-8019.2007.00144.x
21. Li Y, Xia C, Yao G, Zhang X, Zhao J, Gao X, et al, Protective effects of liquiritin on UVB-induced skin damage in SD rats, *Int Immunopharmacol* **97** (2021) 107614; https://doi.org/10.1016/j.intimp.2021.107614
22. Kaur H, Aggarwal G, Nagpal M, Potential benefits of phytochemicals for treatment of hyperpigmentation, *J. Drug Deliv. Ther.* **9**(2) (2019) 420-427; https://doi.org/10.3390/molecules25102422
23. Lin Y, Kuang Y, Li K, Wang S, Song W, Qiao X, et al, Screening for bioactive natural products from a 67-compound library of *Glycyrrhiza inflata*, *Bioorg Med Chem* **25**(14) (2017) 3706-3713; https://doi.org/10.1016/j.bmc.2017.05.009
24. Czajkowska-Kośnik A, Szymańska E, Winnicka K, Nanostructured Lipid Carriers (NLC)-Based Gel Formulations as Etodolac Delivery: From Gel Preparation to Permeation Study, *Molecules* **28**(1) (2022) 235; https://doi.org/10.3390/molecules28010235
25. Iranawati F, Narulitai R, Dewi CSU, Arifin S, editors, Web evaluation of maceration length period on antioxidant potency of *Sonneratia caseolaris* leaf, InE3S Web of Conferences, *EDP Sciences* **153** (2020) 01010
26. Kumari A, Kumar J, Phyto-Chemical Screening of Root Extracts of *Glycyrrhiza Glabra* by Spectroscopic Methods (UV-VIS Spectrophotometer, FTIR & HPLC) *IJPSDR* **11**(6) (2019) 376-381; http://dx.doi.org/10.25004/IJPSDR.2019.110615
27. Yang R, Yuan B-c, Ma Y-s, Zhou S, Zhang H-z, Liu J-y, et al, Simultaneous determination of liquiritin isoliquiritin liquiritigenin and isoliquiritigenin in *Glycyrrhiza uralensis* Fisch. *Glycyrrhiza glabra* L. and *Glycyrrhiza inflata* Bat. by HPLC∗, *Chinese Journal of Pharmaceutical Analysis* **36**(10) (2016) 1729–1736
28. Atapour-Mashhad H, Nejabat M, Hadizadeh F, Hoseinsalari A, Golmohammadzadeh S, Preparation, characterization, and molecular Dynamic Simulation of novel Coenzym Q10 loaded

nanostructured lipid carriers, *Curr Pharm Des* **29**(27) (2023) 2177-2190; https://doi.org/10.2174/1381612829666230911105913
29. Shoviantari F, Erawati T, Soeratri W, Coenzyme Q10 nanostructured lipid carriers as an inducer of the skin fibroblast cell and its irritability test in a mice model, *J Basic Clin Physiol Pharmacol* 2019;**30**(6) (2019) 20190320; https://doi.org/10.1515/jbcpp-2019-0320
30. Castro SR, Ribeiro LNM, Breitkreitz MC, Guilherme VA, Rodrigues da Silva GH, Mitsutake H, et al, A pre-formulation study of tetracaine loaded in optimized nanostructured lipid carriers, *Sci Rep* **11**(1) (2021) 21463; https://doi.org/10.1038/s41598-021-99743-6
31. Kim M-H, Kim K-T, Sohn S-Y, Lee J-Y, Lee CH, Yang H, et al, Formulation and evaluation of nanostructured lipid carriers (NLCs) of 20 (S)-protopanaxadiol (PPD) by Box-Behnken design. *Int. J. Nanomed* (2019) 8509–8520
32. Vaziri MS, Tayarani-Najaran Z, Kabiri H, Nasirizadeh S, Golmohammadzadeh S, Kamali H, Preparation and characterization of Undecylenoyl Phenylalanine loaded-nanostructure lipid carriers (NLCs) as a new α-MSH Antagonist and antityrosinase agent, *Adv Pharm Bull* **13**(2) (2023) 290-300; https://doi.org/10.34172/apb.2023.036
33. Rahmanian-Devin P, Askari VR, Sanei-Far Z, Rahimi VB, Kamali H, Jaafari MR, et al, Preparation and characterization of solid lipid nanoparticles encapsulated noscapine and evaluation of its protective effects against imiquimod-induced psoriasis-like skin lesions, Biomed Pharmacother **168** (2023) 115823; https://doi.org/10.1016/j.biopha.2023.115823
34. Nasirizadeh S, Malaekeh-Nikouei B, Solid lipid nanoparticles and nanostructured lipid carriers in oral cancer drug delivery, *Journal of Drug Delivery Science and Technology* **55** (2020) 101458; https://doi.org/10.1016/j.jddst.2019.101458
35. Chen H, Chang X, Du D, Liu W, Liu J, Weng T, et al, Podophyllotoxin-loaded solid lipid nanoparticles for epidermal targeting, *J Control Release* **110**(2) (2006) 296-306; https://doi.org/10.1016/j.jconrel.2005.09.052
36. Hoseinsalari A, Atapour-Mashhad H, Asili J, Tayarani-Najaran Z, Mohtashami L, Khanavi M, et al, Preparation and Characterization of Nanostructured Lipid Carriers (NLCs) Containing *Glycyrrhiza glabra* Extract for the Treatment of Skin Hyperpigmentation, *Curr Pharm Des* **30**(40) (2024) 3213-3232; https://doi.org/10.2174/0113816128327512240730102545
37. Kalyanaraman B, Darley-Usmar V, Davies KJ, Dennery PA, Forman HJ, Grisham MB, et al, Measuring reactive oxygen and nitrogen species with fluorescent probes: challenges and limitations, *Free Radic Biol Med* **52**(1) (2012) 1-6; https://doi.org/10.1016/j.freeradbiomed.2011.09.030
38. Hadipour E, Tayarani-Najaran Z, Fereidoni M, Vitamin K2 protects PC12 cells against Aβ ((1-42)) and H(2)O(2)-induced apoptosis via p38 MAP kinase pathway, *Nutr Neurosci* **23**(5) (2020) 343-352; https://doi.org/10.1080/1028415x.2018.1504428
39. Qiao Z, Koizumi Y, Zhang M, Natsui M, Flores MJ, Gao L, et al, Anti-melanogenesis effect of *Glechoma hederacea* L. extract on B16 murine melanoma cells, *Biosci Biotechnol Biochem* **76**(10) (2012) 1877–1883; https://doi.org/10.1271/bbb.120341
40. Khumpeerawat P, Duangjinda M, Phasuk Y, Factors affecting gene expression associated with the skin color of black-bone chicken in Thailand, *Poult Sci* **100**(11) (2021) 101440; https://doi.org/10.1016/j.psj.2021.101440
41. Azizsoltani A, Piri K, Behzad S, Soleimani M, Nekouei M, Mahmoudi Z, et al, Ethyl acetate extract of licorice root (*Glycyrrhiza glabra*) enhances proliferation and osteogenic differentiation of human bone marrow mesenchymal stem cells, *Iran J Pharm Res* **17**(3) (2018) 1057–1067

42. Tian M, Yan H, Row KH, Extraction of glycyrrhizic acid and glabridin from licorice, *Int J Mol Sci* **9**(4) (2008) 571–577; https://doi.org/10.3390/ijms9040571
43. Eghlima G, Kheiry A, Sanikhani M, Hadian J, Aelaei M, Nejad Ebrahimi S, Investigation of phytochemical variability, antioxidant activity and ecological conditions of native Iranian *Glycyrrhiza glabra* L. Int. J. Hortic. Sci. **7**(4) (2020) 387-400; https://doi.org/10.22059/ijhst.2020.287117.314
44. Rao H, Ahmad S, Madni A, Rao I, Ghazwani M, Hani U, et al, Compritol-Based Alprazolam Solid Lipid Nanoparticles for Sustained Release of Alprazolam: Preparation by Hot Melt Encapsulation, *Molecules* **27**(24) (2022); https://doi.org/10.3390/molecules27248894
45. Azar FAN, Pezeshki A, Ghanbarzadeh B, Hamishehkar H, Mohammadi M, Nanostructured lipid carriers: Promising delivery systems for encapsulation of food ingredients, *J. Agric. Food Res.* **2** (2020) 100084; http://dx.doi.org/10.1016/j.jafr.2020.100084
46. Izza Nm, Suga K, Okamoto Y, Watanabe N, Bui TT, Wibisono Y, et al, Systematic characterization of nanostructured lipid carriers from cetyl palmitate/caprylic triglyceride/tween 80 mixtures in an aqueous environment, *Langmuir* **37**(14) (2021) 4284-4293; https://doi.org/10.1021/acs.langmuir.1c00270
47. Subramaniam B, Siddik ZH, Nagoor NH, Optimization of nanostructured lipid carriers: Understanding the types, designs, and parameters in the process of formulations, *J. Nanoparticle Res* **22**(6) (2020) 1-29; https://link.springer.com/article/10.1007/s11051-020-04848-0
48. Putranti AR, Primaharinastiti R, Hendradi E, Effectivity and physicochemical stability of nanostructured lipid carrier coenzyme Q10 in different ratio of lipid cetyl palmitate and alpha tocopheryl acetate as carrier, *Asian J Pharm Clin Res* **10**(2) (2017) 146–152; http://dx.doi.org/10.22159/ajpcr.2017.v10i2.14835
49. Danaei M, Dehghankhold M, Ataei S, Hasanzadeh Davarani F, Javanmard R, Dokhani A, et al., Impact of Particle Size and Polydispersity Index on the Clinical Applications of Lipidic Nanocarrier Systems, *Pharmaceutics* **10**(2) (2018) 57; https://doi.org/10.3390/pharmaceutics10020057
50. Hua S, Lipid-based nano-delivery systems for skin delivery of drugs and bioactives, *Front Pharmacol* **6** (2015) 219; https://doi.org/10.3389/fphar.2015.00219
51. Tamjidi F, Shahedi M, Varshosaz J, Nasirpour A, Design and characterization of astaxanthin-loaded nanostructured lipid carriers, *IFSET* **26** (2014) 366-374; http://dx.doi.org/10.1016/j.ifset.2014.06.012
52. Chaturvedi SP, Kumar V, Differential scanning calorimetry as a tool to establish formation of lipid nanoparticles (NLC and SLN), *Res J Pharm Biol Chem Sci* **3**(4) (2012) 1475–1481
53. Gill P, Moghadam TT, Ranjbar B, Differential scanning calorimetry techniques: applications in biology and nanoscience, *J Biomol Tech* **21**(4) (2010) 167–193
54. Daneshmand S, Jaafari MR, Movaffagh J, Malaekeh-Nikouei B, Iranshahi M, Moghaddam AS, et al, Preparation, characterization, and optimization of auraptene-loaded solid lipid nanoparticles as a natural anti-inflammatory agent: In vivo and in vitro evaluations, *Colloids Surf. B Biointerfaces* **164** (2018) 332-339; https://doi.org/10.1016/j.colsurfb.2018.01.054
55. Atapour-Mashhad H, Nejabat M, Hadizadeh F, Hoseinsalari A, Golmohammadzadeh S, Preparation, Characterization, and Molecular Dynamic Simulation of Novel Coenzyme Q10 Loaded Nanostructured Lipid Carriers. *Curr Pharm Des* **29**(27) (2023) 2177-2190; https://doi.org/10.2174/1381612829666230911105913
56. Chmiel T, Mieszkowska A, Kempińska-Kupczyk D, Kot-Wasik A, Namieśnik J, Mazerska Z, The impact of lipophilicity on environmental processes, drug delivery and bioavailability of food components, *Microchemical Journal* **146** (2019) 393-406; https://doi.org/10.1016/j.microc.2019.01.030

57. Farboud ES, Nasrollahi SA, Tabbakhi Z, Novel formulation and evaluation of a Q10-loaded solid lipid nanoparticle cream: in vitro and in vivo studies, *Int J Nanomedicine* **6** (2011) 611-617; https://doi.org/10.2147/ijn.s16815
58. Drygalski K, Siewko K, Chomentowski A, Odrzygóźdź C, Zalewska A, Krętowski A, et al, Phloroglucinol strengthens the antioxidant barrier and reduces oxidative/nitrosative stress in nonalcoholic fatty liver disease (NAFLD), *Oxid Med Cell Longev* **2021**(1) (2021) 8872702; https://doi.org/10.3390/pharmaceutics10020057
59. Gutierrez-Mariscal FM, Arenas-de Larriva AP, Limia-Perez L, Romero-Cabrera JL, Yubero-Serrano EM, López-Miranda J, Coenzyme Q(10) Supplementation for the Reduction of Oxidative Stress: Clinical Implications in the Treatment of Chronic Diseases, *Int J Mol Sci* **21**(21) (2020) 7870; https://doi.org/10.3390/ijms21217870
60. Tippairote T, Bjørklund G, Gasmi A, Semenova Y, Peana M, Chirumbolo S, et al, Combined Supplementation of Coenzyme Q(10) and Other Nutrients in Specific Medical Conditions, *Nutrients* **14**(20) (2022) 4383; https://doi.org/10.3390/nu14204383
61. Hu C, Huang Y, Luo P, Yang Y, Effect of antioxidants coenzyme Q10 and β-carotene on the cytotoxicity of vemurafenib against human malignant melanoma, *Oncol Lett* **21**(3) (2021) 208; https://doi.org/10.3892/ol.2021.12469
62. Gürler EB, Özbeyli D, Buzcu H, Çam ME, Yüksel M, Astaxanthin and Coenzyme Q10 are not synergistic against oxidative damage in cerulein-induced acute pancreatitis, *JOSAM* **5**(3) (2021) 307-310; https://doi.org/10.28982/josam.756220
63. Zhang M, Dang L, Guo F, Wang X, Zhao W, Zhao R, Coenzyme Q10 enhances dermal elastin expression, inhibits IL-1α production and melanin synthesis in vitro, *Int J Cosmet Sci* **34**(3) (2012) 273-279; https://doi.org/10.1111/j.1468-2494.2012.00713.x
64. Gonzalez C, Zegpi C, Noriega V, Prieto JC, Miranda HF, Synergism between dexketoprofen and meloxicam in an orofacial formalin test was not modified by opioid antagonists, *Pharmacol Rep* **63**(2) (2011) 433-440; https://doi.org/10.1016/s1734-1140(11)70509-6
65. Naser A, Albadrany Y, Shaaban K, Isobolographic analysis of analgesic interactions of silymarin with ketamine in mice, *J Hellenic Vet Med Soc* **71**(2) (2020) 2171-2178
66. Tallarida RJ, Stone DJ, Jr., Raffa RB, Efficient designs for studying synergistic drug combinations, *Life Sci* **61**(26) (1997) Pl 417-425; https://doi.org/10.1016/s0024-3205(97)01030-8
67. Sohail M, Rakha A, Butt MS, Asghar M, Investigating the antioxidant potential of licorice extracts obtained through different extraction modes, *J. Food Biochem.* **42**(2) (2018) e12466; http://dx.doi.org/10.1111/jfbc.12466
68. Hseu Y-C, Ho Y-G, Mathew DC, Yen H-R, Chen X-Z, Yang H-L, The in vitro and in vivo depigmenting activity of Coenzyme Q10 through the down-regulation of α-MSH signaling pathways and induction of Nrf2/ARE-mediated antioxidant genes in UVA-irradiated skin keratinocytes, *Biochem Pharmacol* **164** (2019) 299-310; https://doi.org/10.1016/j.bcp.2019.04.015